Excitable laser processing network node in hybrid silicon: analysis and simulation

Mitchell A. Nahmias, Alexander N. Tait, Bhavin J. Shastri, Thomas Ferreira de Lima, and Paul R. Prucnal

11. S. Beri, L. Mashall, L. Gelens, G. Van der Sande, G. Mezosi, M. Sorel, J. Danckaert, and G. Verschaffelt, "Excitability in optical systems close to z2-symmetry," Phys. Lett. A **374**, 739–743 (2010).
12. M. A. Nahmias, B. J. Shastri, A. N. Tait, and P. R. Prucnal, "A leaky integrate-and-fire laser neuron for ultrafast

(ORNoC): Architecture and design methodology," in "Design, Automation Test in Europe Conference Exhibition (DATE), 2011," (2011), pp. 1–6.
41. D. G. Feitelson, *Optical Computing: A Survey for Computer Scientists* (MIT Press, USA, 1988).

1. Introduction

Recently, there has been a surge of interest in the hybridization of photonic and electronic physics to achieve unique processing capabilities. In this context, there has been significant research in using laser dynamics for both information processing [1–3] and communication [4,5]. Multiplexing in optical networks have also been exploited for similar gains in performance [6, 7]. A more specific approach involves studying the dynamical property of excitability in lasers, in which discrete pulses are generated in response to perturbations that exceed a threshold [8–11]. Excitable lasers can process information in a way that resembles spiking in biological neuron models. In comparison, however, lasers can exhibit dynamics roughly eight orders of magnitude faster while being mathematically isomorphic to their biological counterparts [12].

In this manuscript, we simulate a unified, realistic model of a reconfigurable excitable laser processor, recently proposed in [13]. This model includes a detailed analysis and simulation of a processing-network node (PNN) as defined in a recent laser networking scheme [14]. Although parts of the signal pathway have been proposed [13–15], no single model has fully characterized the signal pathway of a PNN. The device uniquely allows for a large fan-in (10s to 100s per unit) without routing or packet switching, and utilizes the ultrafast dynamics of lasers for high bandwidth (GHz) processing. We describe the photonic circuit techniques used in our approach and simulate the device based on experimentally measured parameters in a standard hybrid III-V/silicon platform [16]. The model allows us to explore critical properties such as energy consumption, cascadability, and signal bandwidth, and verifies that the PNN can be fabricated in a realistic device structure.

Spiking neural networks (SNNs)—systems whose communication channels code information in events rather than bits—have received significant attention as an alternative to the von Neumann paradigm of computation. Hardware SNNs take advantage of distributed, sparse, and robust coding schemes to perform computations to minimize size, weight and power, and have been utilized both as biological network simulators and low-power data processors.

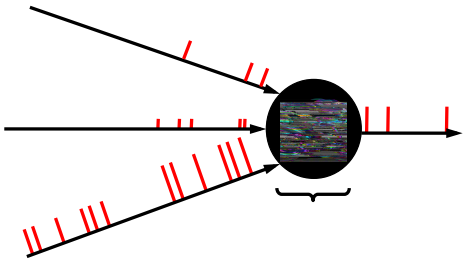

Fig. 1. (a) A general depiction of a processor in a SNN. Input channels are weighted by w_i,

novel information encoding/retrieval through the direct modulation of carrier waveforms.

2. Methods

As illustrated in Fig. 2, the PNN consists of three primary components: reconfigurable spectral filters, photodetectors, and an excitable laser. Although an inhibitory photodetector is shown in the schematic diagram, the behavior of the devices are similar, aside from a reversal of the ground and signal pads. In this analysis, we only examine the excitatory photodetector pathway for brevity and conciseness. In this scheme, WDM spike signals arrive along a dedicated waveguide. Weights are applied to each channel via a set of tunable spectral filters.

Inputs from other laser neurons are weighted in the optical domain before reaching the photodetector. The photodetectors produce a photocurrent summing the total optical power. Demultiplexing many input channels is not necessary because the incoherent sum of all WDM channels is intentionally computed by the photodetector. The photodetectors receive optical pulses from a network and produce a current signal which modulates the laser carrier injection. The excitable laser performs nonlinear discrimination and regenerates the pulsed signal, analogous to the neural axon hillock. The photodetector front-end proposed here allows for significant signal fan-in, while tunable filters allow adjustments of the weights between neurons, allowing for network reconfigurability.

2.1. Technology Platform

We describe an instantiation of the PNN in the hybrid/III-V platform. This platform includes

Fig. 2. (Top) A depiction of an LIF neuron with a synaptic variable, embedded within a network. (Bottom) A schematic of the proposed laser neuron, complete with filters, balanced photodetectors, and an excitable laser. In this model, only the excitatory photodetector pathway is investigated.

and choose d_{tun} = 4:4 (0.66 nm) and Dd = 8:8 (1.3 nm) to achieve tolerable levels of the extinction ratio, crosstalk and insertion loss [14]. A filter bank will receive a series of pulses from other lasers, each governed by some output power function $P_{out[j]}(t)$ for neuron j at an associated wavelength l_j.

There is also a linewidth associated with the output of each laser. Single mode distributed feedback (DFB) lasers, the structures assumed here, tend to have narrow linewidths. Nonethe-

j will take the form:

$$S_{in[j]}(\lambda;t) = \sum_i T_{ij}(\lambda) S_{out[i]}(\lambda;t) \tag{3}$$

where $T_{ij}(\lambda)$ is the transmission function of ring i for neuron j. Therefore, for a given photodetector spectral responsivity linear system R_λ, the current produced by the photodetector is as follows:

$$i_{p[j]}(t) = \sum_i \int_\lambda R_\lambda \quad T_{ij}(\lambda) S_{out[i]}(\lambda;t) \quad d\lambda \tag{4}$$

Based on our assumptions, we can approximate the filter linewidth as significantly larger than the signal bandwidth.The 40 ps $sech^2$ pulses used in this simulation have transform-limited bandwidth of $\Delta\lambda = .42$ (.063 nm), which is much smaller than the bandwidth of the filters (as shown in Fig. 4(b)), allowing this approximation to be valid. We assume the photodetector response is approximately spectrally flat over the C-band [31], and neglect carrier diffusion limitations to frequency response, which are small compared to the RC limitations included in this model. This allows us to approximate the responsivity as a constant $R_{\lambda_i}\{P(t)\} = R_{PD}P(t)$. Therefore, we can simplify the photodiode current to the following expression:

$$i_{p[j]}(t) \quad \sum_{i} R_{PD} P(t) \int_{\lambda} T_{ij}(\lambda)$$

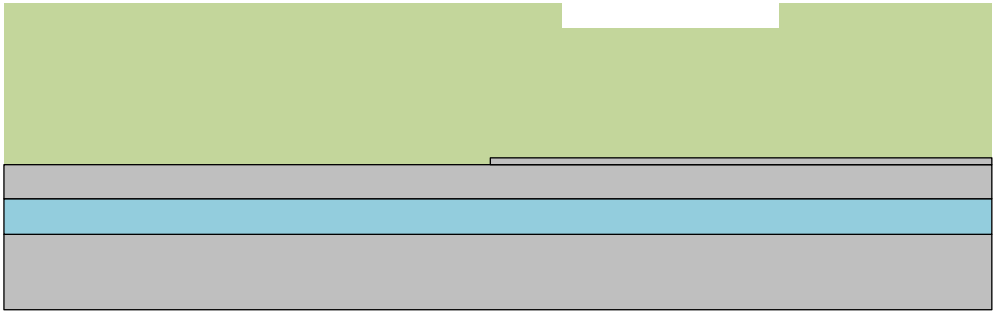

Fig. 3. Cross section of the device and full modeling structure for the hybrid silicon/III-V laser neuron (inhibitory photodetector not included). A series of pulses along n different wavelength channels $\lambda_1 ::: \lambda_N$ are spectrally filtered (i.e. weighted). This results in an excitatory photodetector current response, which propagates into the equivalent circuit depicted above. The interaction between the photons in the cavity, gain and SA sections are modeled using rate equations. The resulting output power along wavelength λ_j becomes the input to other neurons in a given network.

where F is the linear transfer function of the modeled circuit.

A simulation of multiple input pulses is shown in Fig 5. The laser is pumped with a stable current source I_p, while the PD is reverse biased with a large voltage (>5 V) to offset the influence of I_p. Responsivity is assumed to be $0.81 A/W$ [16]. The junction is kept fairly short (100s of μm) to avoid transmission line effects.

While the general expression for the complex impedance of the link is more involved, in practice, the dominant parasitics are the capacitance of the metal wire C_p and the contact resistances R_{PD}, R_L. The metal wire capacitance C_p is the easiest to adjust lithographically, either by changing the height of the oxide layer or the area occupied by the metal bridge to change the characteristics of the junction.

A common first order model for synaptic dynamics is an integrator with decay [35]:

$$\frac{ds}{dt} = \frac{s}{\tau} + I(t)$$

where $I(t)$ is the input, τ is the time constant and $s(t)$ is the synaptic variable. A neuron will typically sum signals from multiple synapses $s_i(t)$ and receive them as inputs. In biological systems, synaptic variables typically represent neurotransmitter concentrations. In our case, it represents the RC charged signal. This behavior takes place independently of temporal integra-

Table 1. Hybrid/III-V Laser Parameters

series Param.	series Description	series Value
V_g	gain section volume	1.68 10 ^{11} cm^3
V_a	SA section volume	3.36 10 ^{12} cm^3
G	QW conf. factor	0.056
n_0	transparency carrier density	1.75 10^{18} cm ^{3}
v_g		

Under a desired parameter regime, the internal dynamics can be compressed so that pulse generation is instantaneous. The behavior simplifies to [12]:

$$\frac{dG(t)}{dt} = g_G(G(t) \quad A) + q(t); \qquad \text{(8a)}$$

$$\text{if } G(t) > G_{\text{thresh}}$$

assumed to have a faster lifetime, which helps improve the dynamics and consistency of the input signals [13]. The equations can be simplified to the undimensionalized set of equations through a set of variable substitutions [12, 38]. The results are shown in Fig. 5.

The output power of laser

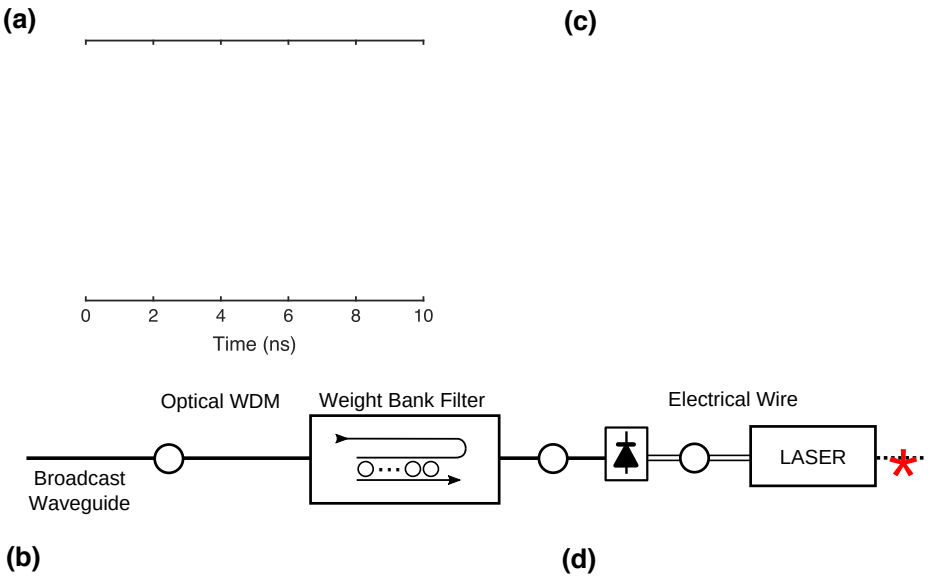

Fig. 4. Simulation of the response of the processing network node at each step. (a) Input WDM spike signals coming from the broadcast waveguide with FWHM = 40 ps. Trace color indicates the carrier wavelength of each pulse. (b) Transmission of spectrum of the weight bank filter (dotted lines) and input signal power spectra (solid curves). Input signals are assumed to be at the transform limit for 10 ps pulses. (c) WDM signals after transmission through the filter bank. Pulses on the same wavelength channel acquire the same weight and are then detected. (d) Electronic current signal, $i_e(t)$, that modulates the laser neuron after traversing the parasitic circuit model in Fig. 3. Pulses are low pass filtered to FWHM = 56 ps after traveling through device parasitics.

3. Discussion

The model developed in this paper—including the filter bank, electrical junction, and laser neuron—enables the exploration of both analog signal properties and the effect of physical design decisions on the behavior of networked PNNs. An example simulation of the complete model with WDM optical-in and optical-out is shown in Figs. 4 and 5. The front-end weight bank and photodetector in Figs. 4(a)–4(c) act to generate an electronic representation of the weighted sum of WDM inputs carrying FWHM=40 ps pulses. This signal that modulates the laser neuron is shown in Fig. 4(d), after traversing the parasitic circuit model from Fig. 3. While some pulse spreading is visible (FWHM=56 ps), pulse amplitude and timing information is clearly maintained when realistic parasitic values are used. Figure 5 illustrates the internal dy-

#246538 Received 22 Jul 2015; revised 15 Sep 2015; accepted 22 Sep 2015; published 2 Oct 2015

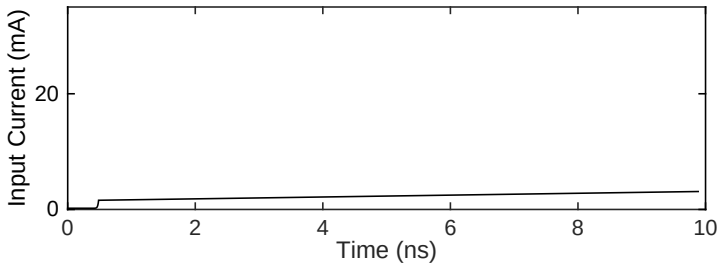

Fig. 5. Simulated internal dynamics of the laser neuron in response to the modulation signal in Fig 4.d. (a) input electrical modulation $i_e(t)$ (black line) causes the release of a large

computing [41]. At the same time, the temporary conversion to the electrical domain does not significantly degrade the signal, as this work has simulated. Every device in the primary signal pathway performs both physical and computational roles, resulting in a robust, ultrafast, and efficient signal pathway.

Utilization complementary physics along the signal pathway is not unlike this pathway in biological neurons, in which electrical action potentials are converted to chemical signals called neurotransmitters upon reaching a synapse (the junction between neurons). Chemical signaling is a relatively short-range process, but it introduces much more functionality compared to direct electrical modulation (e.g. both excitation and inhibition, a variety of synaptic timeconstants,